Anti-Windup Compensator Design for Fixed-Tilt Multirotors with Interaction Capabilities

Dharani JAYANNA[1,a *], Davide INVERNIZZI[1,b], Daniele MAGLIORE[2,c], Simone PANZA[2,d], and Marco LOVERA[1,e]

[1]Dipartimento di Scienze e Tecnologie Aerospaziali, Politecnico di Milano, Via La Masa 34, 20156 Milano, Italy

[2]ANT-X s.r.l., Via Davanzati 33, 20158 Milano, Italy

[a]dharani.jayanna@polimi.it, [b]davide.invernizzi@polimi.it, [c]daniele@antx.it, [d]simone@antx.it, [e]marco.lovera@polimi.it

Keywords: Anti-Windup Synthesis, Fully-Actuated UAVs, Aerial Physical Interaction, Actuator Saturation, Lateral Force Constraints

Abstract. This work addresses actuator saturation in fixed-tilt multirotor platforms used for aerial interaction. The fixed-tilt configuration imposes lateral force limitations, and exceeding these bounds under external disturbances can degrade performance and stability. To mitigate this, an anti-windup (AW) compensator is synthesized via an LMI-based convex optimization framework derived from the linearized closed-loop dynamics. An external wrench observer is integrated to estimate and counteract interaction and aerodynamic disturbances. The proposed AW augmented compensator structure preserves local stability during saturation, achieving improved transient behavior in simulation on the ARIES tiltrotor platform.

Introduction

The design of control strategies for aerial robots operating under constrained actuation has gained significant attention as unmanned aerial vehicles (UAVs) evolve from purely observational tasks to platforms capable of physical interaction for inspection and maintenance tasks [1]. Within this context, fully actuated multirotors have emerged as a promising class of vehicles capable of generating independent force and torque vectors in all degrees of freedom, enabling versatile interaction capabilities [2]. Among these, the fixed-tilt configuration stands out as one of the most structurally minimal designs, achieving full actuation through a non-coplanar arrangement of propellers. However, such a configuration introduces inherent lateral force constraints, since the available horizontal forces depend on the fixed cant and dihedral angles, which are typically chosen to satisfy nominal interaction requirements [2]. Under external influences such as contact interactions or wind disturbances, the controller may demand forces beyond the feasible envelope, leading to actuator saturation that degrades tracking performance and can compromise stability.

To address these limitations, this work presents the design of an anti-windup (AW) compensator providing stability guarantees under actuator saturation [3]. The compensator is synthesized through a convex optimization procedure based on linear matrix inequalities (LMIs), formulated from the linearized closed-loop dynamics of the system around a nominal equilibrium. The resulting design approximates the ideal unsaturated performance while maintaining stability within the feasible control region. In addition, an external observer is incorporated to reconstruct the forces and torques acting on the multirotor, thereby compensating for the reaction effects arising from contact interactions and aerodynamic disturbances. The synthesized AW compensator is integrated with both the dynamic feedback controller and the external observer to prevent wind-up phenomena. The proposed framework is validated in simulation, demonstrating effective suppression of wind-up and improved closed-loop behavior compared to the baseline controller.

UAV Dynamics and Control Architecture

The experimental platform considered in this study is the ARIES tiltrotor, developed by ANT-X s.r.l. [4]. ARIES is a fixed-tilt hexarotor, as illustrated in Fig. 1, designed for aerial interaction and contact-based inspection tasks, capable of maintaining stable flight while exerting forces on the environment.

Figure 1: ARIES fixed-tilt hexarotor.

The motion of the hexarotor is described by the standard six-degree-of-freedom Newton-Euler equations. The translational dynamics are expressed in the inertial frame $\mathcal{F}_I = (O_I, i_1, i_2, i_3)$, while the rotational motion is represented in the body-fixed frame $\mathcal{F}_B = (O_B, b_1, b_2, b_3)$, centered at the platform's center of mass. Here, i_j and b_j $(j \in 1,2,3)$ denote right-handed orthonormal bases of the inertial and body frames, respectively, and O_I, O_B are their corresponding origins. The resulting dynamics are expressed as:

$$m\dot{v}_I = -mg\mathbb{e}_3 + R(f_{ca} + f_r), \quad J\dot{\omega}_B = -\omega_B \times J\omega_B + \tau_{ca} + \tau_r, \tag{1}$$

where $m \in \mathbb{R}_{>0}$ and $J = J^T \in \mathbb{R}^{3\times3}_{>0}$ denote the platform mass and inertia matrix, $R \in \mathrm{SO}(3)$ is the body-to-inertial rotation matrix, and v_I, ω_B are the translational and angular velocities defined in $\mathcal{F}_I$ and $\mathcal{F}_B$ frames respectively. The propeller generated wrench $w_{ca} = [f_{ca}^T \quad \tau_{ca}^T]^T$ acts on the vehicle, while the external wrench $w_r = [f_r^T \quad \tau_r^T]^T$ models aerodynamic and contact effects. The desired control wrench $w_c = [f_c^T \quad \tau_c^T]^T$ is mapped to the individual rotor thrusts through the constant input matrix $\mathbb{F}(\alpha, \beta) \in \mathbb{R}^{6\times6}$, defined by the geometry of the ARIES platform [5]:

$$w_c = \mathbb{F}(\alpha, \beta)\left[k_f\omega_1^2 \quad \dots \quad k_f\omega_6^2\right]^T, \qquad R_B^{R_i} = R_Y(\beta_i)R_X(\alpha_i)R_Y(\beta_a)R_Z(\psi_i),$$
$$\mathbb{F}_i(\alpha_i, \beta_i) = \begin{bmatrix} -R_{R_i}^B\mathbb{e}_3 \\ \left(-\left[x_{BR_i}^B\right]_\times + (-1)^{i-1}k_f^\tau \mathrm{I}_3\right) R_{R_i}^B\mathbb{e}_3 \end{bmatrix}, \tag{2}$$

where $\alpha, \beta \in \mathbb{R}^6$ are cant and dehidral angles of each propeller. Fully actuated multirotors allow independent force and torque control, enabling diverse feedback designs such as geometric or linear control [1, 6]. A hierarchical cascade structure is adopted, with outer position and attitude loops and inner velocity and rate loops. The translational controller computes f_c, while the attitude controller determines τ_c, yielding:

$$f_c = m\left(K_{vp}R\left(K_{pp}(p_r - p_I) + v_r - v_I\right) - K_{vd}R\dot{v}_I\right) - mgR\mathbb{e}_3 - \hat{f}_r,$$
$$\tau_c = K_{\omega p}\left(K_{\theta p}(\Theta_r - \Theta_B) + \omega_r - \omega_B\right) - K_{\omega d}\dot{\omega}_B - \hat{\tau}_r, \tag{3}$$

where $K_{(\cdot)} \in \mathbb{R}^{3\times3}_{\geq0}$ are diagonal gain matrices and the vectors p_r, v_r, Θ_r, and ω_r represent the desired position, velocity, attitude, and angular rate setpoints, respectively. The observer-estimated wrench $\hat{w}_r = [\hat{f}_r^T \quad \hat{\tau}_r^T]^T$ compensates the external effects w_r in Eq. 1. The commanded wrench w_c is distributed through $\mathbb{F}(\alpha, \beta)$ in Eq. 2, ensuring accurate force and torque generation within the actuator range. When the compensated command exceeds feasible actuation, the applied wrench w_{ca} deviates from w_c, related by:

$$w_{ca} = \mathrm{sat}_{[u^-,u^+]}(w_c), \quad \mathrm{sat}_{[u^-,u^+]}(u) = \max\{\min\{u^+, u\}, -u^-\}, \tag{4}$$

where the saturation acts component-wise, with bounds $u^-, u^+ \in \mathbb{R}^{n_u}_{\geq0}$ and input dimension $n_u \in \mathbb{N}$. The next section introduces the external observer that estimates the acting wrench and integrates with the control framework.

Materials Research Proceedings 69 (2026) 794-799 https://doi.org/10.21741/9781644904251-140

External Wrench Observer

Accurate estimation of external forces and moments is crucial for safe aerial interaction, especially when direct sensing is impractical due to payload or hardware constraints. To reconstruct the external wrench acting on the platform, a model-based observer [6] is formulated using the UAV dynamics and onboard inertial measurements. The translational and rotational estimators are defined respectively as:

$$\begin{aligned} m\dot{\hat{v}}_I &= mg\mathbb{e}_3 + R^T\left(\mathbb{F}_f k_f \omega^2 + \hat{f}_r\right) + \Lambda_v(v_I - \hat{v}_I), \qquad \dot{\hat{f}}_r = \Lambda_f R(v_I - \hat{v}_I), \\ J\dot{\hat{\omega}}_B &= -\omega_B \times J\omega_B + \mathbb{F}_\tau k_\tau \omega^2 + \hat{\tau}_r + \Lambda_\omega(\omega_B - \hat{\omega}_B), \quad \dot{\hat{\tau}}_r = \Lambda_\tau(\omega_B - \hat{\omega}_B), \end{aligned} \tag{5}$$

where $\hat{v}_I$ and $\hat{\omega}_B$ are the estimated linear and angular velocities, and $\hat{f}_r$, $\hat{\tau}_r$ represent the estimated external force and torque. The positive definite gain matrices $\Lambda_{(\cdot)} \in \mathbb{R}^{3\times 3}_{\geq 0}$ govern estimator dynamics, balancing responsiveness and noise sensitivity. Matrices $\mathbb{F}_f$ and $\mathbb{F}_\tau$ map rotor speeds to translational and rotational components of the applied control wrench as mentioned in Eq. 1. This observer reconstructs external wrench in real time without dedicated sensors, enhancing disturbance compensation; however, when the estimated forces drive control inputs beyond actuator limits, an anti-windup compensator is augmented as discussed in the next section.

Anti-Windup Compensator Synthesis

The nonlinear dynamics of the multirotor, along with the baseline controller and external wrench observer, are linearized around the hovering equilibrium corresponding to zero attitude and steady thrust balancing gravity. The resulting augmented linear model captures the coupled behavior of the plant, controller, and observer, forming the basis for the AW synthesis. Following the methodology of [3], a fixed-structure AW compensator is introduced by embedding additional feedback gains within the controller to preserve stability under actuator saturation. The overall closed-loop system used for AW synthesis can be expressed in compact form as:

$$\begin{cases} \dot{\xi} = A\xi + B_q q_X, \\ z_e = C_z\xi + D_{zq} q_X, \\ y_c = C_y\xi + D_{yq} q_X, \end{cases} \tag{6}$$

Where $\xi = [x_a^T \quad x_{rm}^T \quad w^T]^T$ denotes the augmented closed-loop state, comprising the plant, controller, external wrench observer, and AW compensator states. The reference model represents the ideal system with unconstrained actuation, while w belongs to a specified class of reference inputs. The performance variable is $z_e = z - z_{rm}$, i.e., the deviation between the saturated response and the nominal reference-model output. The signal q_X denotes the AW interconnection term capturing the difference between the controller command and its saturated counterpart.

Based on this representation, the AW synthesis problem aims to determine the compensator gains that minimize the ℓ_2-norm of the performance output z_e, ensuring Lyapunov-based stability within a prescribed region of attraction. The resulting optimization problem is cast as a convex program subject to LMI constraints, whose solution directly yields the AW gain matrices. For detailed derivations and proofs, the reader is referred to [3].

Simulation Results

The closed-loop architecture of the ARIES platform incorporating the AW compensator is depicted in Fig. 2. The baseline controller generates the desired control wrench w_c from the reference signals y_r and w, while the external observer estimates the reaction wrench $\hat{w}_r$ using the measured states y and applied wrench w_{ca}. The control command is mapped through $\mathbb{F}^{-1}$, constrained by actuator limits via the saturation nonlinearity, and subsequently redistributed to the plant through $\mathbb{F}$. The AW compensator processes the input mismatch q_X between the pre and post saturation signals to synthesize the corrective term v_{AW}, which is fed back to both the controller and observer to ensure consistent dynamic behavior and stability within the saturation region.

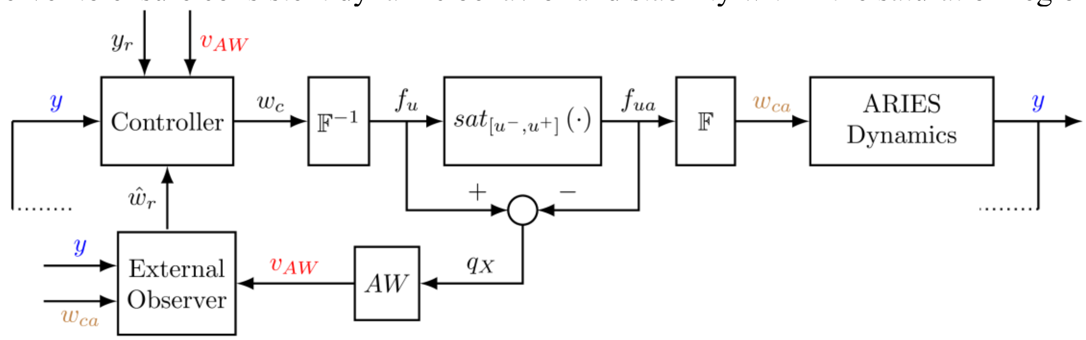

Figure 2: ARIES AW-augmented closed-loop system.

The proposed control framework is validated in simulation using the ARIES dynamic model, where the platform is commanded to maintain a hovering condition while subjected to a step-like external disturbance designed to induce actuator saturation. The simulations evaluate the capability of the AW-augmented controller to preserve stability and tracking accuracy under saturation, demonstrating the compensators effectiveness in mitigating windup effects and maintaining consistent closed-loop performance.

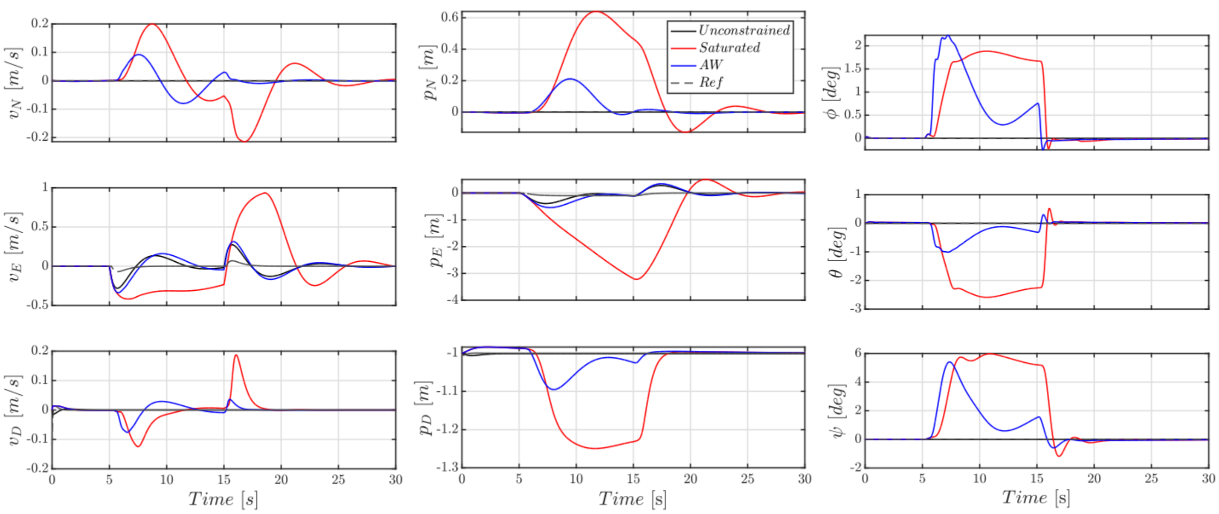

Figure 3: Position (left), velocity (middle), and attitude (right) tracking performance for fixed-tilt hexarotor under various controllers.

Fig. 3 illustrates the position, velocity, and attitude tracking performance of the fixed-tilt hexarotor under three configurations: the unconstrained nominal controller, the saturated controller without compensation, and the proposed AW-augmented controller. When saturation occurs, the nominal controller exhibits significant deviation and oscillatory behavior, particularly in the lateral and yaw dynamics, indicating loss of stability. In contrast, the AW-compensated response closely follows the nominal trajectory, achieving smooth transient behavior and faster recovery once the actuators re-enter the feasible region.

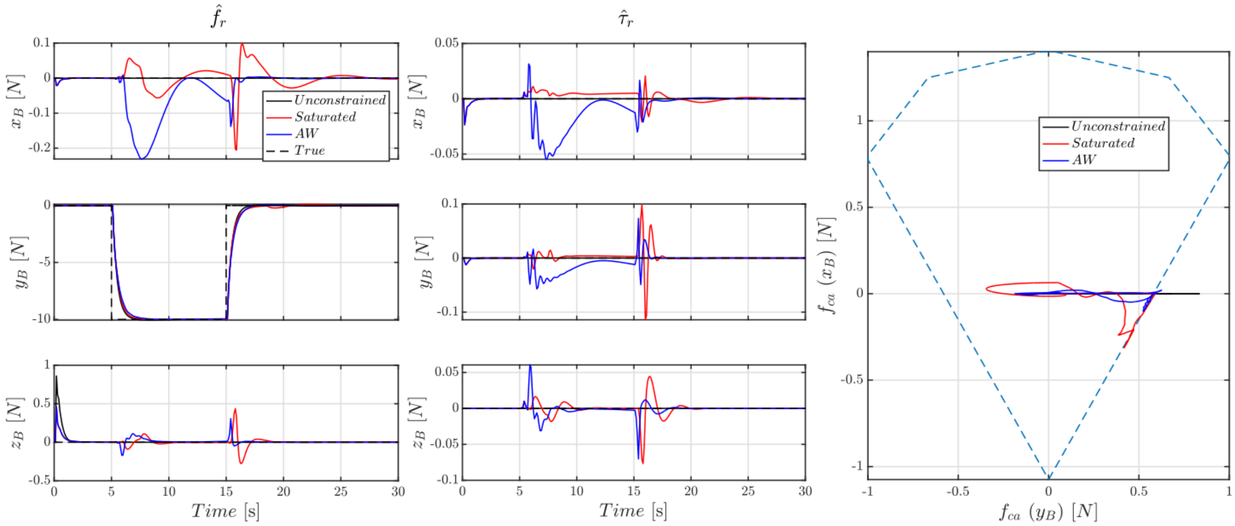

Figure 4: Estimated force (left), torque (middle), and applied force (right) with respect to available force envelope under various controllers (axes scaled for confidentiality).

Fig. 4 presents the estimated force and torque components, along with the applied force envelope in the lateral plane. The AW-compensated controller effectively limits the commanded forces within the feasible actuation range while maintaining consistent disturbance rejection. The force trajectories remain tangent to the saturation boundary, demonstrating how the compensator ensures stable recovery from saturation without inducing excessive overshoot or steady-state bias. These results confirm that the proposed anti-windup strategy effectively preserves nominal control performance within the feasible actuation region while ensuring stable and robust behavior under saturation-induced nonlinearities.

Summary

This work presents an anti-windup compensator for fixed-tilt multirotors operating under actuator saturation and external interaction forces. The framework integrates a model-based external wrench observer with a performance-oriented compensator synthesized through convex LMI optimization. Simulations on the ARIES hexarotor show that the AW-augmented controller mitigates windup, maintaining stability and near-nominal tracking under severe actuation limits. Future efforts will extend the approach to experimental validation for contact interaction scenarios.

Acknowledgement

This work is supported by the European Union - NextGenerationEU under the National Recovery and Resilience Plan (PNRR), Mission 4, Component 2 “From Research to Enterprise” - Investment 3.3, within the framework of the doctorate program activated under Ministerial Decree No. 352 of 9/04/2022.

References

[1] R. Rashad, J. Goerres, R. Aarts, J. B. Engelen, and S. Stramigioli, Fully actuated multirotor uavs: A literature review, IEEE Robotics and Automation Magazine, vol. 27, no. 3, pp 97-107, 2020. https://doi.org/10.1109/MRA.2019.2955964

[2] D. Kotarski, P. Piljek, J. Kasać, and D. Majetić, Performance analysis of fully actuated multirotor unmanned aerial vehicle configurations with passively tilted rotors, Applied Sciences, vol. 11, no 18, p. 8786, 2021. https://doi.org/10.3390/app11188786

[3] P. Ghignoni, N. Buratti, D. Invernizzi, and M. Lovera, Anti-windup design for directionality compensation with application to quadrotor uavs, IEEE Control Systems Letters, vol. 5, no. 1, pp. 331-336, 2020. https://doi.org/10.1109/LCSYS.2020.3001881

[4] ANT-X s.r.l., Aries - industrial drone for aerial interaction, https://antx.it/industrial-drones-antx/aries/, accessed: November 6, 2025.

[5] M. Ryll, H. H. Bülthoff, and P. R. Giordano, Modeling and control of a quadrotor uav with tilting propellers, in 2012 IEEE international conference on robotics and automation. IEEE, 2012, pp. 4606-4613. https://doi.org/10.1109/ICRA.2012.6225129

[6] M. Ryll, G. Muscio, F. Pierri, E. Cataldi, G. Antonelli, F. Caccavale, D. Bicego, and A. Franchi, 6d interaction control with aerial robots: The flying end-effector paradigm, The International Journal of Robotics Research, vol. 38, no. 9, pp. 1045-1062, 2019. https://doi.org/10.1177/0278364919856694